*Korean J. Chem. Eng.*, 33(3), 812-822 (2016)
DOI: 10.1007/s11814-015-0218-4

pISSN: 0256-1115
eISSN: 1975-7220

# Application of Ni-doped ZnO rods for the degradation of an azo dye from aqueous solutions

**Mitra Gholami*, Mehdi Shirzad-Siboni*,†, and Jae-Kyu Yang****

*Department of Environmental Health Engineering, School of Public Health, Iran University of Medical Sciences, Tehran, Iran
**Division of General Education, Kwangwoon University, Seoul 01899, Korea
(*Received 12 July 2015 • accepted 14 October 2015*)

**Abstract**−Ni-doped ZnO rods were applied as a photocatalyst for the degradation of an azo dye (Reactive Black 5). Effects of solution pH, catalyst dosage, initial RB5 concentration, $H_2O_2$ concentration, different purging gases, and type of organic compounds on the removal efficiency of RB5 were studied. Ni-doped ZnO rods were synthesized by co-precipitation method. Neutral pH was selected as an optimal pH condition due to a photo-corrosion of ZnO in acidic and basic conditions. Photocatalytic degradation efficiency of RB5 was increased as the catalyst dosage increased up to 1 g/L, while it was decreased by increasing initial RB5 concentration. Pseudo-first-order rate constant ($k_{obs}$) decreased from 0.122 to 0.0051 $min^{-1}$ and electrical energy per order ($E_{Eo}$) increased from 39.34 to 941.18 ($kWh/m^3$) by increasing RB5 concentration from 5 to 100 mg/L, respectively. Photocatalytic degradation efficiency of RB5 increased by increasing $H_2O_2$ concentration, but this trend was not observed above 10 mM. Photocatalytic degradation efficiency of RB5 increased in the presence of folic acid and citric acid while interference was observed in the presence of humic acid, EDTA, oxalic acid, and phenol. Photocatalytic activity was maintained even after five successive cycles.

Keywords: Synthesis, Ni-doped ZnO Rods, Reactive Black 5, Catalyst, Kinetic Models

## INTRODUCTION

Synthetic dyes used in textile industries are important pollutants in water systems [1-5]. Azo compounds having one or more azo groups (-N=N-) in aromatic rings are a kind of synthetic dye commonly used for coloring agents in the textile, paint, ink, plastics, and cosmetics industries [6]. Among several azo dyes, reactive dyes have azo-based with different reactive groups [7,8]. They are widely used in the textile industries because of their simple drying procedure and good stability during the washing process [7]. Remazol Black B (reactive black 5) has very toxic, mutagenic, little biodegradability, and carcinogenic properties [9]. Thus, reactive black 5 should be treated with suitable treatment processes such as electrocoagulation [9], adsorption [10], membrane process [11], wet oxidation [12], and bioremediation [13]. Among several processes, advanced oxidation processes (AOPs) producing hydroxyl radicals via UV/$H_2O_2$, UV/$O_3$, UV/ZnO, UV/$TiO_2$, and UV/Fenton process have been widely used for the removal of toxic compounds [9,14-16]. ZnO and $TiO_2$ are commonly used for their easy availability and nontoxicity [14,17-19].

Zinc oxide (ZnO) is a semiconductor having a wide band gap energy (~3.3 eV) that has transparent properties in the visible range [20-22]. However, there are some limitations in the application of pure ZnO particles as a photocatalyst. One main limitation is the fast recombination rate of the generated electron and positive hole [23]. Therefore, reduction of electron-hole recombination rate is highly necessary for the real application of pure ZnO particles [23]. Usually, ZnO is doped with different types of metallic ions such as Sn, Ga, In, Sn, Al, Sc, and Y in order to improve its transparent conducting oxide (TCO) property [24-28]. Doping of transition metal ions on the ZnO lattice can modify its optical, electrical, and magnetic properties [12,24-26]. A number of studies have been reported for the improvement of optical and magnetic properties of ZnO by doping of transition metal ions [29]. Saharan et al. [26] used Ni doped ZnO nanoparticles and ultrasonication in photocatalytic degradation of Victoria blue (VB) and Fast green FCF (FG) dyes [26]. Kaneva et al. [30] investigated the effect of nickel doping on the photocatalytic activity of ZnO thin films under UV and visible light for removal of Malachite Green (MG) [30]. Kant and Kumar [24] investigated photocatalytic properties of ZnO and Ni doped ZnO nanospheres prepared by sol-gel method for removal of Methylene Blue (MB) [24]. Also, there are many reports about photocatalytic degradation of dyes with undoped ZnO [1, 31-33]. However, very little information is available for the removal efficiency and removal kinetics of RB5 with illuminated Ni doped ZnO particles at different reaction parameters.

We used a modified synthetic method of Ni-doped ZnO compared to the other researchers. Saharan et al. [26] synthesized Ni-ZnO via chemical precipitation method by using surfactant CTAB at low temperature [26]. Kant and Kumar [24] used citric acid for the preparation of Ni doped ZnO nanospheres by sol-gel method [24]. Applicability of Ni-doped ZnO rods as an efficient photocatalyst for the degradation of RB5 was evaluated at different reaction conditions. Effect of initial solution pH, photocatalyst dosage, initial RB5 concentration, $H_2O_2$ concentration, different purging gases, and different type of organic compounds (folic acid, citric

†To whom correspondence should be addressed.
E-mail: mshirzadsiboni@yahoo.com, shirzad.m@iums.ac.ir

**Table 1. Chemical structure and characteristics of RB5**

| Color index name | Reactive black 5 |
|---|---|
| Chemical structure | 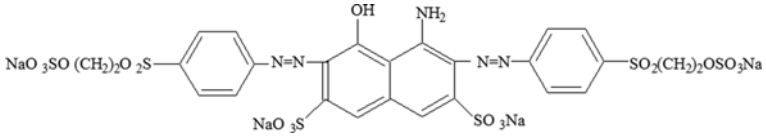 |
| Chemical class | Anionic, Diazo |
| Molecular formula | $C_{26}H_{21}Na_4N_5O_{19}S_6$ |
| Color index number | 20505 |
| $\lambda_{max}$ (nm) | 597 |
| $M_w$ (g/mol) | 991.8 |
| Reactive group | Sulfatoethylsulfone |
| $pK_a$ | 5.8 |

acid, humic acid, oxalic acid, phenol, ethylenediaminetetraaceticacid (EDTA)) on the photocatalytic degradation of RB5 was investigated. Additionally, kinetic study was conducted and experimental results were simulated with zero, first, second, and Langmuir-Hinshelwood kinetic models. The electrical energy per order ($E_{Eo}$) was calculated to evaluate the cost-efficiencies of the applied processes.

## MATERIALS AND METHODS

### 1. Chemicals

Zinc nitrate, nickel nitrate, acetone, sodium hydroxide, folic acid, citric acid, humic acid, oxalic acid, phenol, EDTA, hydrogen peroxide, and hydrochloric acid were purchased from Merck, Germany, and used without further purification. Reactive Black 5 (RB5) was purchased from Alvan Sabet Co., Iran. Chemical structure and absorption spectrum of RB5 at different pHs are presented in Table 1 and Fig. 1, respectively [10]. A photocatalytic reactor used in previous work was applied in this study [34]. A 125 W medium-pressure UVC lamp (Arda, France), emitting maximum wavelength at 247.3 nm, was applied as a light source. The light intensity of UVC lamp was equal to 1,020 μw/cm$^2$ measured by a Spectroline model DRC-100X digital radiometer combined with a DIX-365 radiation sensor (ShokofanTosee, Iran).

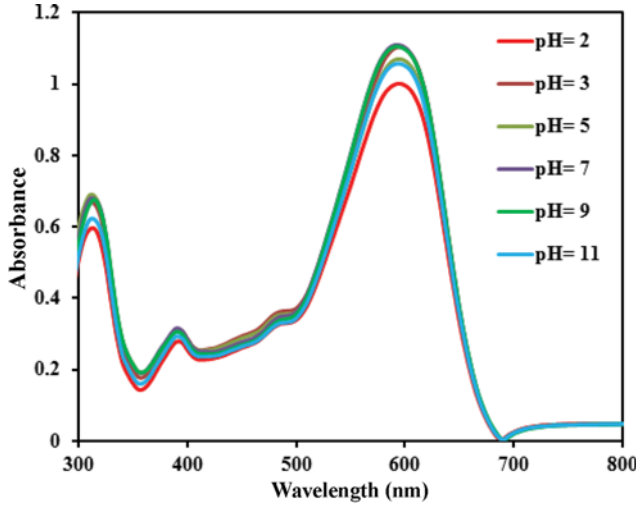


**Fig. 1. The absorption spectrum of reactive black 5 at different pHs.**

### 2. Synthesis of ZnO Sheets and Ni-doped ZnO Rods by Co-precipitation Method

ZnO sheets were synthesized adopting the method previously reported [34]. A stock solution (pH=6) of 0.1 M Zn(II) was prepared by dissolving zinc chloride into distilled water. Then 0.2 M NaOH solution was added dropwise to the precursor solution to obtain an alkaline medium (pH=12), producing a white and gelatinous ZnO. The synthetic reaction was fundamentally performed for 7 h under constant stirring. The solid products in aqueous solution were centrifuged (Sigma-301, 4,000 rpm, Germany), washed with deionized water, and then dried at 100 °C for 3 h. Ni-doped ZnO powder was synthesized using a co-precipitation method. Zn(II) and Ni(II) solutions were prepared by dissolving appropriate amount of zinc nitrate ($Zn(NO_3)_2{\cdot}6H_2O$) and nickel nitrate ($Ni(NO_3)_2{\cdot}6H_2O$) into distilled water, respectively. The nickel nitrate solution was slowly added to the zinc nitrate solution under constant stirring. Ammonia solution (0.2 M) was added dropwise to the precursor solution to obtain an alkaline medium (pH 10) producing green color precipitates. Then the solutions were mixed for 3 h under constant stirring. The solid products in aqueous solution were centrifuged (Sigma-301, 4,000 rpm, Germany), washed five times with distilled water, three times with acetone, and then dried for 18 h at 80 °C. Finally, the sample was calcined at 250 °C. Fourier transform infrared spectroscopy (FT-IR), X-ray diffraction (XRD), field emission scanning electron microscopy (FE-SEM), energy dispersive X-ray spectroscopy (EDX), X-ray photoelectron spectroscopy (XPS), Raman spectroscopy (Jobin-Yvon, HR800) with the 514 nm line of an Ar ion laser, and UV-Vis spectrophotometer (Hach-DR 5000, USA) were used to characterize the prepared ZnO particles and Ni-doped ZnO rods. The $pH_{ZPC}$ of Ni-doped ZnO rods was determined adopting the method previously reported [35].

### 3. Experimental Procedure and Analysis

A stock solution (1,000 mg/L) of RB5 was prepared by dissolving RB5 into distilled water. In each experiment, a certain dosage of the photocatalyst (0.1-1 g/L) was added in 1 L of RB5 solution at different concentration (5-100 mg/L) and solution pH (3-11).

The initial pH of solution was adjusted by adding NaOH or HCl (0.1 mol/L) and was measured by pH meter (Metron, Switzerland). All experiments were performed for 2 h. The solution in the photoreactor was kept at constant temperature (25±1 °C) and constantly stirred. The photocatalyst suspension was equilibrated in the dark for 15 min. After equilibration, the UV-lamp was switched on and a portion of suspension (10 mL) was removed at definite time intervals. The aqueous sample was centrifuged (Sigma-301, Germany) at 4,000 rpm for 10 min to eliminate photocatalyst and then the concentration of residual RB5 was analyzed. The RB5 concentration in each sample was measured with a spectrophotometer (UV/Vis Spectrophotometer, Hach-DR 5000, USA) at $\lambda_{max}$=597 nm by a calibration curve, which was obtained based on Beer-Lambert law [36]. Chemical oxygen demand (COD) was determined by COD reactor model AR851 (HACH, USA) according to the Standard Methods [36].

## RESULTS AND DISCUSSION

### 1. Characterization of Photocatalyst

1-1. FT-IR Analysis

The functional groups on the surface of photocatalyst can play a significant role in the photocatalytic activity, because photocatalytic reactions mostly occur on the surface of photocatalyst. Thus, FT-IR analysis on the surface of ZnO sheets and Ni-doped ZnO rods was performed in the range of 400-4,000 $cm^{-1}$ (Fig. 2(a) and (b)). FT-IR spectrum showed several significant absorption peaks at 458, 727, 913, 1,512, 1,608, 2,889, and 3,451 $cm^{-1}$ for the ZnO sheets and absorption peaks at 425, 553, 886, 1,382, 1,630, and 3,388 $cm^{-1}$ for the Ni-doped ZnO rods. The band located at 458 $cm^{-1}$ corresponds to Zn-O stretching. The band at 3,500 $cm^{-1}$ corresponds to the hydroxyl groups ($^{-}$OH). In the FT-IR spectrum of the Ni-doped ZnO rods, the broad absorption bands at 3,451 $cm^{-1}$ and 3,388 $cm^{-1}$ correspond to the O-H stretching vibration of water present in ZnO, and the other absorption band at 2,889 $cm^{-1}$ may

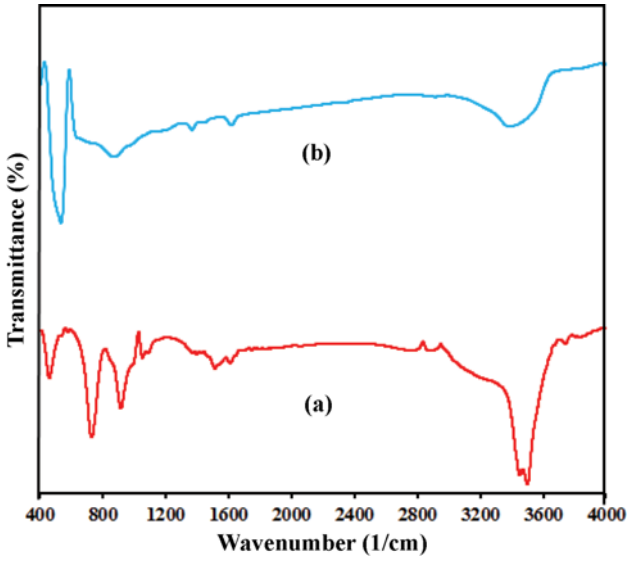


**Fig. 2. FT-IR image of samples: (a) ZnO sheets and (b) Ni-doped ZnO rods.**

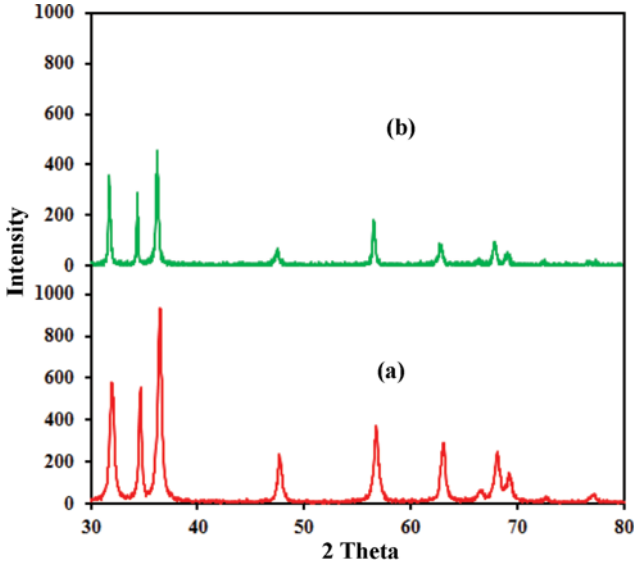


**Fig. 3. XRD image of samples: (a) ZnO sheets and (b) Ni-doped ZnO rods.**

be assigned to a residual organic component [26,35]. The bands at 1,608 $cm^{-1}$ and 1,630 $cm^{-1}$ can be associated with the bending vibration of $H_2O$ molecules. The stretching bands at 485 $cm^{-1}$ and 425 $cm^{-1}$ confirm the formation of ZnO particles [26]. The peaks between 400 and 600 $cm^{-1}$ are assigned to metal-oxygen (M-H) stretching mode [25]. FT-IR spectra of Ni doped ZnO are almost similar to those of ZnO. The vibration modes at 886 and 1,382 $cm^{-1}$ are associated with $Ni^{2+}$ occupation at $Zn^{2+}$ sites [25].

1-2. XRD Analysis

Fig. 3(a) and (b) show the X-ray diffraction patterns of ZnO sheets and Ni-doped ZnO rods, respectively. The dominant peaks of ZnO sheets depicted as $2\theta$ values are 31.68, 34.32, 36.13, 47.48, 56.50, 62.80, 66.54, 67.88, 69.07, 73.00 and 77.34°, corresponding to the (100), (002), (101), (102), (110), (103), (200), (112), (201), (004) and (202) planes of hexagonal wurtzite ZnO according to JCPDS Card number of 36-1451, respectively [37]. In addition, as shown in Fig. 3(b), peaks corresponding to nickel oxides or other crystalline material were not found in the recorded patterns. While, decreased peak intensities were observed due to substitution of Ni ion into ZnO matrix [28]. This result indicates that nickel ions have been successfully replaced in ZnO lattice. The average grain size of ZnO sheet and Ni-doped ZnO rods was 21.23 nm and 14.23 nm for ZnO sheets and Ni-doped ZnO rods, respectively, by using Scherrer's equation [29]. It is generally known that direct replacement of the lattice ion by the dopant metal occurs if the size of the dopant ion is comparable or smaller compared to that of lattice ion [38].

1-3. SEM and EDX Analysis

Field emission scanning electronic microscopy (FE-SEM) images of ZnO and Ni-doped ZnO rods were analyzed by a Mira microscope (Mira3, Tescan, Czech Republic). SEM images of ZnO sheets and Ni-doped ZnO rods are shown in Fig. 4(a) and Fig. 4(b), respectively. Fig. 4(a) and (b) show sheet structure of ZnO and rod structure of Ni-doped ZnO, respectively. EDX patterns of the ZnO

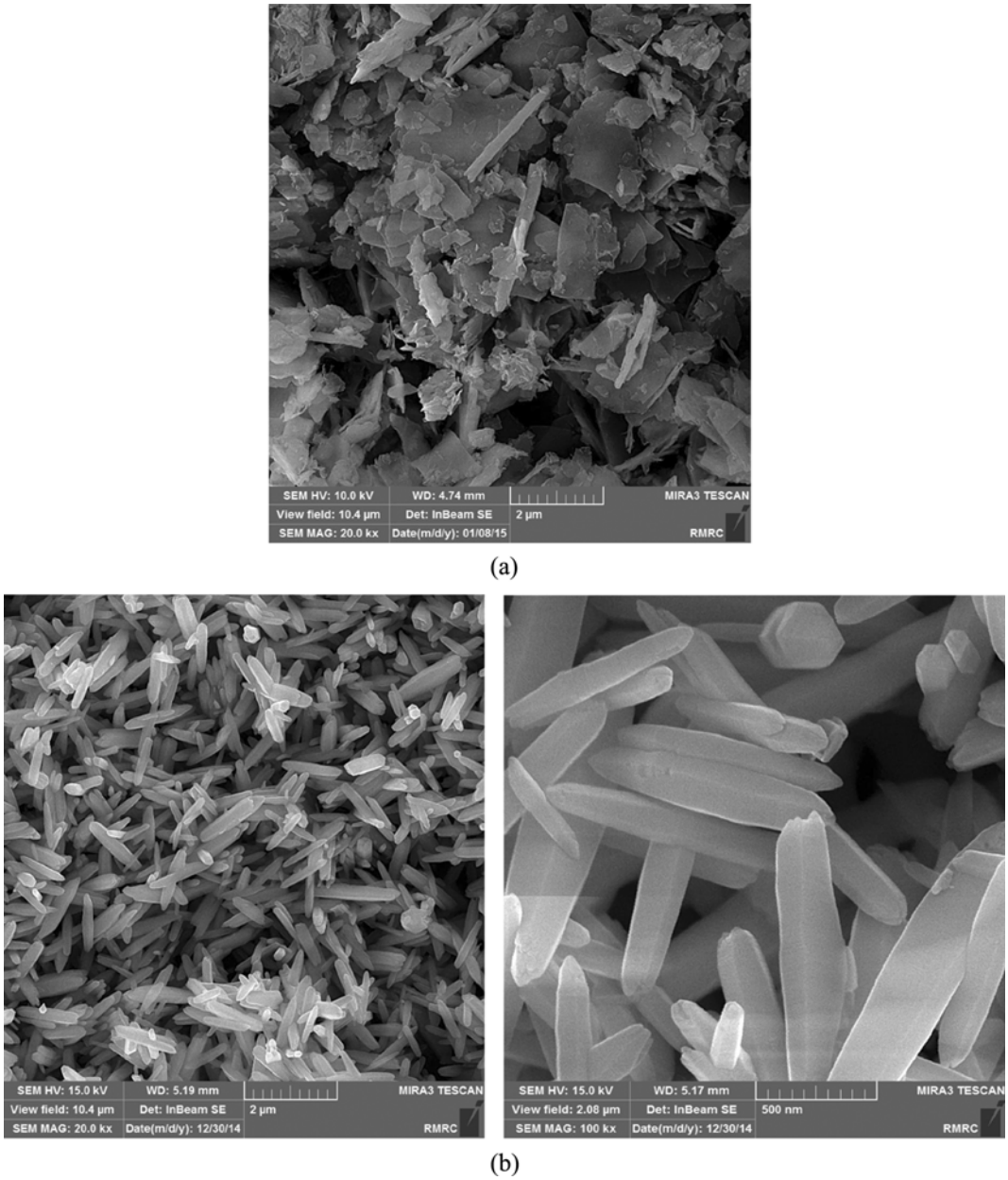


**Fig. 4. SEM image of samples: (a) ZnO sheets and (b) Ni-doped ZnO rods.**

sheets and Ni-doped ZnO rods are depicted in Fig. 5(a) and (b), respectively. According to the results of EDX analysis, weight percent of Zn and O in the ZnO sheets was 57.28 and 42.72%, and weight percent of Zn, O, and Ni in the Ni-doped ZnO rods was 47.47, 35.16 and 1.7%, respectively. Therefore, the synthesized compound is composed of Zn, O, and Ni, indicating formation of Ni-doped ZnO rods.

1-4. XPS, Raman and UV-Vis Analysis

XPS, Raman, and UV-Vis images of ZnO sheets and Ni-doped ZnO rods are shown in Fig. 6(a), Fig. 6(b), and Fig. 6(c), respectively. Valance state, substitution, and content of Ni ions in ZnO rods are shown in the XPS spectrum. The peaks of Ni $2p_{3/2}$ and Ni $2p_{1/2}$ core levels are found at 855.51±0.10 and 873.01±0.10 eV, respectively, whereas the corresponding satellite structures are clearly observed at 861.014±0.10 and 879.214±0.10 eV [39,40]. The Ni $2p_{3/2}$ (855.51±0.10 eV) position is quite different from that of metallic Ni (852.7 eV), NiO (853.8 eV), and $Ni_2O_3$ (856.7 eV) [39]. This indicates that nickel of Ni-doped ZnO rods is present as +2 valence state [39,40]. Therefore, it is likely that there is a replacement of $Zn^{+2}$ by $Ni^{+2}$ in the ZnO lattice [39,40]. Fig. 6(b) displays the Raman spectra of ZnO sheets and Ni-doped ZnO. Raman spectra showed significant absorption peaks at 335, 382, 445, and 578 $cm^{-1}$ for the ZnO sheets and absorption peaks at 342, 395, 447, and 583 $cm^{-1}$ for the Ni-doped ZnO rods [39]. Also, the peak intensity (445 $cm^{-1}$) of Ni-doped ZnO rods has been decreased due to doping of Ni into ZnO matrix [39]. Two additional modes were appeared at 528 and 816 $cm^{-1}$ after doping, which was associated with the lattice defect [39].

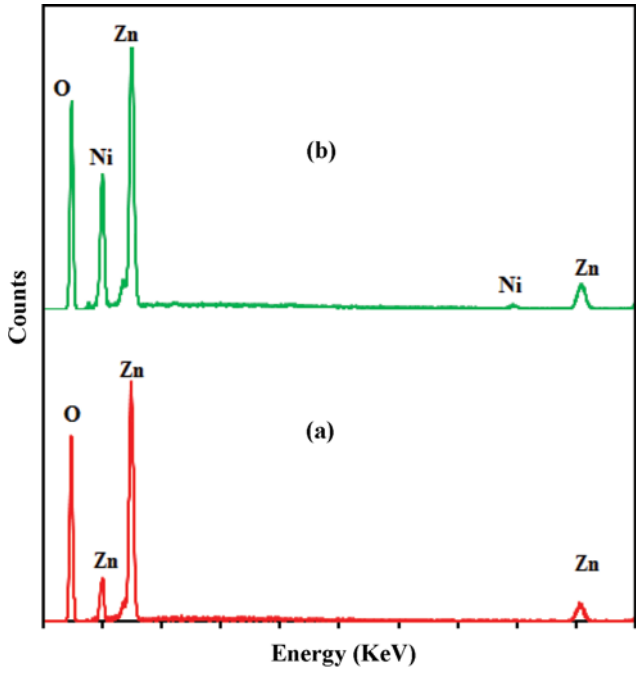


**Fig. 5. EDX image of samples: (a) ZnO sheets and (b) Ni-doped ZnO rods.**

Effect of Ni substitution on wurtzite structure of ZnO was further confirmed using UV-visible optical spectroscopy measured in the range 300-800 nm. Fig. 6(c) shows optical absorption spectra of ZnO sheets and Ni-doped ZnO rods. The absorption band edge of undoped ZnO was observed at 360 nm and it shifted to longer wavelength region (375 nm) for the Ni-doped ZnO rods [41]. The observed red shift in the absorption band edge with nickel doping in ZnO may be due to the *sp-d* exchange interactions between the band electrons and the localized *d*-electrons of the $Ni^{2+}$ ions [41]. Such a red shift in band edge with increasing nickel dopant is a clear indication of the incorporation of Ni ions into the Zn site of the ZnO matrix [41].

**2. Effects of Operational Parameters on the Photocatalytic Degradation of RB5**

2-1. Effect of Initial pH on the Photocatalytic Degradation of RB5

Effect of initial pH on the photocatalytic degradation of RB5 with illuminated Ni-doped ZnO rods was investigated by varying the initial pH from 3 to 11 at constant dosage of photocatalyst (0.2 g/L) and at constant initial RB5 concentration (20 mg/L). Fig. 7 shows that degradation efficiency of RB5 was enhanced from 77.46 to 91.35% by increasing the initial pH from 3 to 7 and then decreased to 80.53% at pH 11. One reason for the maximum degradation efficiency at neutral pH can be the photo-corrosion of ZnO in strong acidic and basic solutions. The $pH_{pzc}$ of Ni-doped ZnO rods was approximately 8. The $pH_{pzc}$ of ZnO is known as 9 from previous studies [42]. The surface of Ni-doped ZnO rods acquires a negative surface charge above pH 8 [1,37]. However, below $pH_{ZPC}$, the surface of Ni-doped ZnO rods acquires positive charge, and dye molecule also has a little negative charge. Therefore, there is weak attraction between dye molecule and Ni-doped ZnO rods that causes decreasing dye uptake. Since the most effec-

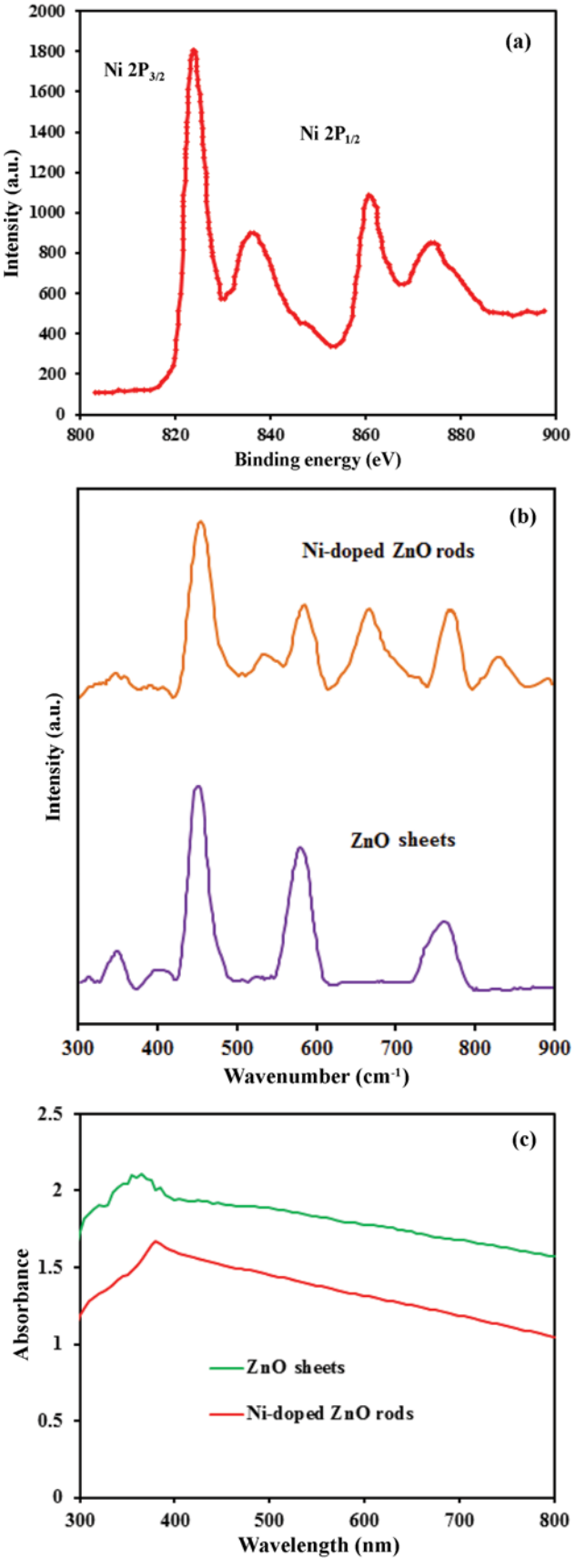


**Fig. 6. (a) XPS for Ni-doped ZnO rods, (b) Raman, and (c) UV-Vis image of samples.**

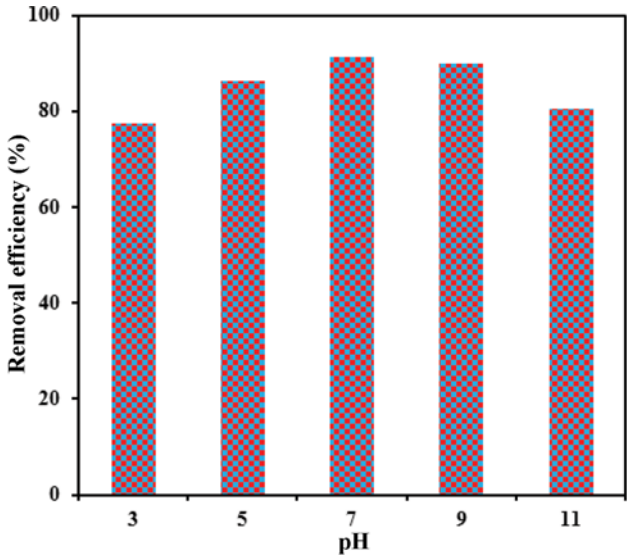


**Fig. 7. The effect of initial pH on the photocatalytic degradation of RB5 (catalyst dosage=0.2 g/L, $[RB5]_0$=20 ppm).**

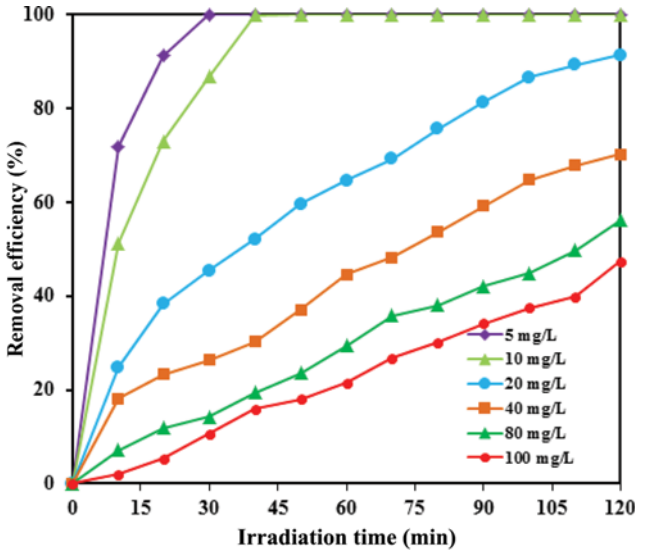


**Fig. 9. The effect of initial RB5 concentration on the photocatalytic degradation of RB5 (catalyst dosage=0.2 g/L, pH=7).**

tive degradation of RB5 was observed at pH 7, other experiments were also performed at the same pH [1]. Also, stability of Ni-doped ZnO rods has been assessed at different solution pH values. According to the $pH_{pzc}$ data, the results showed that Ni-doped ZnO rods are stable in acidic solutions (pH>2).

2-2. Effect of Photocatalyst Dosage

Effect of photocatalyst dosage on the photocatalytic degradation of RB5 was studied by varying the Ni-doped ZnO rods dosage (0.1, 0.2, 0.4, 1 g/L) at constant concentration of RB5 (20 mg/L) and at pH 7. Fig. 8 shows that initial adsorption efficiency at time zero, without UV irradiation, varied from 5.48 to 32.74% depending on the dosage of Ni-doped ZnO rods. The increased total active surface area can be a major reason for the enhanced removal of RB5. Since the photocatalytic degradation efficiency of RB5 was just slightly different between 0.2 g/L and 1 g/L (almost 8.64%), further experiments were performed at 0.2 g/L. Photocatalytic degradation efficiency of RB5 increased from 24.83 to 91.35% by increasing irradiation time from 15 to 120 min in Ni-doped ZnO rods dosage equal to 0.2 g/L.

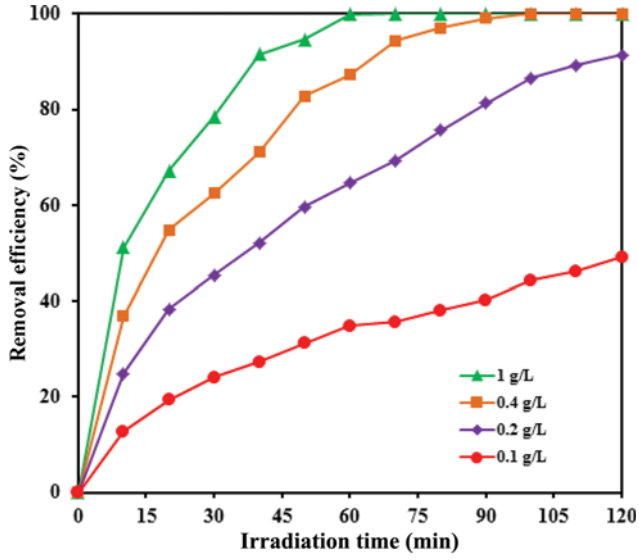


**Fig. 8. The effect of catalyst dosage on the photocatalytic degradation of RB5 (pH=7, $[RB5]_0$=20 ppm).**

2-3. Effect of Initial Concentration of RB5

Removal of RB5 by UV/Ni-doped ZnO rods was investigated by varying the initial RB5 concentration (5, 10, 20, 80, 80, 100 mg/L) at initial pH 7 and at constant Ni-doped ZnO rods (0.2 g/L) (Fig. 9). Photocatalytic degradation efficiency of RB5 decreased from 99.99 to 47.41% with increasing initial RB5 concentration from 5 to 100 mg/L after 2 h. When the initial RB5 concentration increased, more RB5 molecules could be adsorbed on the surface of Ni-doped ZnO rods. The large amount of adsorbed RB5 and its degradation intermediates might have an inhibitive effect on the further photocatalytic degradation of RB5, because only a few free sites are available on the surface of Ni-doped ZnO rods for receiving photons [31,32]. Moreover, when RB5 concentration increases, it causes more absorption of UV light causing inner filtration effect. Similar results have been reported [17,18,43,44].

2-4. Effect of the Hydrogen Peroxide

Photocatalytic removal of RB5 has been studied at different hydrogen peroxide concentrations from 2 to 50 mM at constant initial RB5 concentration (20 mg/L), photocatalyst dosage (0.2 g/L), and pH7 for 120 min. As shown in Fig. 10, photocatalytic degradation efficiency of RB5 increased up to 10 mM but decreased above 10 mM. The increased removal efficiency of RB5 after addition of $H_2O_2$ below 10 mM can be explained by the increased reaction between $H_2O_2$ and electron in the conduction band of Ni-doped ZnO rods, causing effective inhibition of electron-hole recombination as described in Eq. (2) [32,33,37]. Since hydrogen peroxide is a better electron acceptor than dissolved oxygen, it can act as a good electron acceptor during photocatalytic reaction at low concentration. While, at high concentration, it can act as a powerful scavenger of •OH as shown in Eqs. (4) and (5), causing a

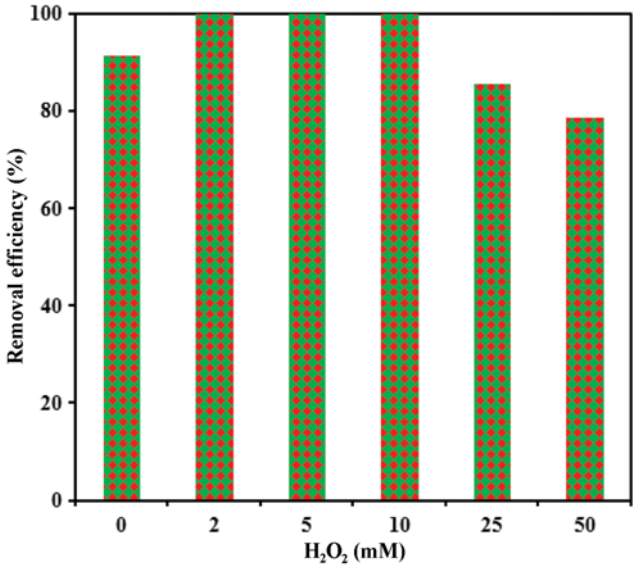


**Fig. 10. The effect of hydrogen peroxide on the photocatalytic degradation of RB5 (catalyst dosage=0.2 g/L, pH=7, $[RB5]_0$= 20 ppm).**

decrease of the photocatalytic degradation efficiency of RB5 [33,37]. Daneshvar et al. [32] reported that removal efficiency AO7 in UV/ZnO process increased with increasing $H_2O_2$ concentration, but the improvement was not obvious above 10 mM [32].

$$H_2O_2+e^-_{CB}\rightarrow OH^-+HO^{\cdot} \quad (1)$$

$$H_2O_2+h\upsilon\rightarrow 2HO^{\cdot} \quad (2)$$

$$H_2O_2+HO^{\cdot}\rightarrow HO_2^{\cdot}+H_2O \quad (3)$$

$$HO_2^{\cdot}+HO^{\cdot}\rightarrow H_2O+O_2 \quad (4)$$

$$H_2O_2+h^+_{VB}\rightarrow H^++HO_2^{\cdot} \quad (5)$$

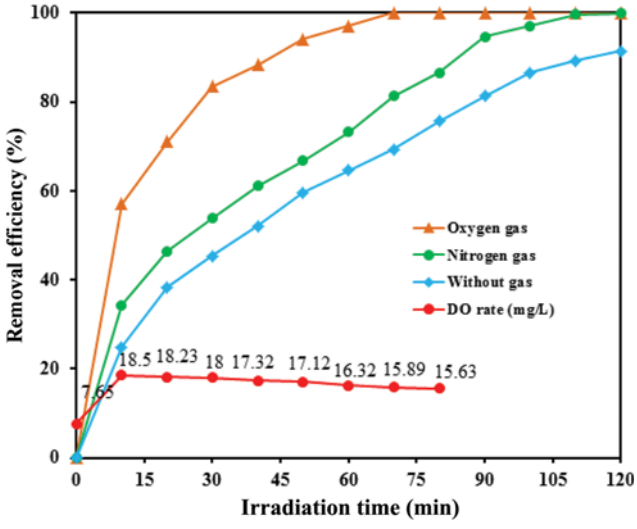


**Fig. 11. The effect of different purging gases and variation of DO concentration during photocatalytic degradation of RB5 (catalyst dosage=0.2 g/L, pH=7, $[RB5]_0$=20 ppm).**

These results suggest that proper addition of hydrogen peroxide is necessary in order to accelerate the photocatalytic degradation rate of RB5.

2-5. Effect of Purging Gas

Fig. 11 shows the effect of different purging gases such as nitrogen and oxygen on the photocatalytic degradation of RB5. In this experiment, initial RB5 concentration, photocatalyst dosage, and initial pH were 20 mg/L, 0.2 g/L and 7, respectively. The gas flow rate was 2 L/min. Photocatalytic degradation efficiency of RB5 was enhanced with purging of both nitrogen gas and oxygen gas compared to that at ambient condition. The photocatalytic degradation efficiency of RB5 with oxygen purging increased from 57.0 to 99.99% as reaction time increased from 10 to 80 min. The photocatalytic degradation efficiency of RB5 with nitrogen purging increased from 34.3 to 99.91% as reaction time increased from 10 to 120 min. However, it ranged from 24.83 to 91.35% by increasing time from 10 to 120 min at ambient condition. Also, the dissolved oxygen concentration was measured over the reaction time. As shown in Fig. 11, the dissolved oxygen concentration decreased from 18.5 to 15.63 mg/L as reaction time increased from 10 to 80 min. This result indicates the important role of oxygen during photocatalysis [45]. Dissolved oxygen can be transformed to a superoxide radical anion ($^{\cdot}O_2^-$), which can produce reactive radicals through several reaction steps by reaction with excited electrons in the conduction band of photocatalysts [45]. Another reason for the enhanced photocatalytic degradation of RB5 with gas purging may be the increased electron scavenging effect. Electrons generated in the conduction band may effectively react with dissolved oxygen, which can inhibit recombination between positive holes and electrons [46]. Also, the COD was measured over the reaction time. The COD value at 0, 15, 30, 45, 60, 75, 90, 105, 120 min was 800, 300, 260, 200, 180, 120, 100, 50, 50 mg/L, respectively. Percentage of COD removal increased from 62.5 to 93.75%. Saharan et al. [26] reported that presence of oxygen gas increased the removal efficiency of Victoria blue (VB) and Fast green FCF (FG) due to the synergistic effect of Ni doped ZnO nanoparticles and ultrasonication, but it decreased in the presence of argon gas [26]. Chakrabarti and Dutta [47] reported photocatalytic degradation of Eosin Y and Methylene Blue dyes in wastewater using ZnO as a photocatalyst [47]. The result showed that the percentage degradation of Eosin Y increased from 39 to 63% as the air flow rate increased from 0 to 11.3 L/min. Corresponding COD removal increased from 8.1 to 37.8%. For Methylene Blue, COD removal increased from 50 to 58% as the airflow rate increased from 0 to 6.13 L/min. Percentage of COD removal increased from 20 to 24%. Pare et al. [48] reported that purging of oxygen gas increased removal efficiency of Lissamine Fast Yellow (LFY) in ZnO suspension, but it decreased with $N_2$ purging [48].

2-6. Effect of the Presence of Organic Compounds

To assess the effect of different organic compounds on the photocatalytic degradation of RB5, constant amounts of organic compounds (folic acid, citric acid, humic acid, oxalic acid, phenol, ethylenediaminetetraacetic acid (EDTA)) were added to the photocatalytic reactor. Initial concentration of each organic compound was 20 mg/L. And initial concentration of RB5, photocatalyst dosage, and initial pH was 20 mg/L, 0.2 g/L, and 7, respectively. Fig.

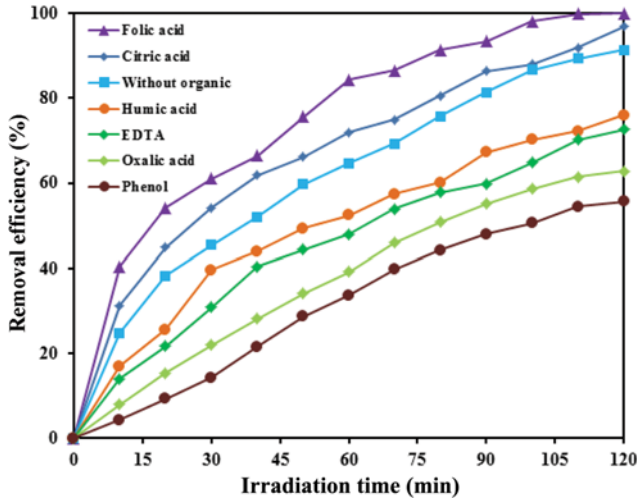


**Fig. 12. The effect of different organic compounds on the photocatalytic degradation of RB5 (catalyst dosage=0.2 g/L, pH=7, $[RB5]_0$=20 ppm, organic compounds=20 ppm).**

12 shows that RB5 removal increased in the presence of folic acid and citric acid compared to the control test (without organic species). However, RB5 removal decreased in the presence of humic acid, EDTA, oxalic acid and phenol. The increased photocatalytic degradation of RB5 in the presence of folic acid and citric acid can be attributed to the production of additional oxidants during photocatalytic oxidation of folic acid and citric acid [49]. But the decreased photocatalytic degradation of RB5 in the presence of humic acid, EDTA, oxalic acid and phenol can be attributed to the greater interference effect of adsorbed organic molecules on the surface of photocatalyst than production of additional oxidants.

### 3. Kinetics and Electrical Energy Per Order ($E_{Eo}$) Studies

To obtain kinetic information, experimental results were fitted with zero, first- and second-order equations [45]. To obtain kinetic data for the photocatalytic degradation of RB5, $[RB5]_0-[RB5]_t$, $\ln[[RB5]_0/[RB5]_t]$, and $1/[RB5]_t-1/[RB5]_0$ versus t was plotted at different initial RB5 concentrations. The relationship between initial degradation rate (r) and initial RB5 concentration for a heterogeneous photocatalytic degradation process can be described by Langmuir-Hinshelwood model. From economic point of view, the $E_{Eo}$ value of the photocatalytic degradation of RB5, defined as the number of kWh of electrical energy required to reduce pollutant concentration by 1 order of magnitude (90%) in 1 $m^3$ of contaminated water, was evaluated. Equations and constants are summarized in Table 2.

**Table 3. Kinetic parameters and electrical energy per order obtained at different RB5 concentration (catalyst dosage=0.2 g/L and pH=7)**

| $[RB5]_0$ (ppm) | First-order | | $R^2$ | Electrical energy per order |
|---|---|---|---|---|
| | $k_{obs}$ ($min^{-1}$) | $1/k_{obs}$ (min) | | $E_{Eo}$ (kWh/$m^3$) |
| 5 | 0.122 | 8.19 | 0.9995 | 39.34 |
| 10 | 0.0666 | 15.01 | 0.9986 | 72.07 |
| 20 | 0.017 | 58.82 | 0.9879 | 282.35 |
| 40 | 0.0098 | 102.04 | 0.9876 | 489.80 |
| 80 | 0.0065 | 153.84 | 0.9866 | 738.46 |
| 100 | 0.0051 | 196.07 | 0.9841 | 941.18 |

Photocatalytic degradation of RB5 was fitted well with the pseudo-first order kinetic model compared to the other kinetic models. As can be seen from Table 3, pseudo-first order rate constants ($k_{obs}$) and $R^2$ decreased from 0.122 to 0.0051 $min^{-1}$ and 0.9995 to 0.9841 with increasing the initial RB5 concentration from 5 to 100 mg/L. The $k_{obs}$ values for each initial concentration (Table 3) were calculated from the slope between $\ln[[RB5]_0/[RB5]_t]$ versus reaction time. $K_{RB5}$ and $k_c$ were 0.241 (L/mg) and 0.524 (mg/L/min) by plotting $1/k_{obs}$ versus initial RB5 concentration, respectively. Daneshvar et al. [32] reported L-H equation constants for degradation of Acid Orange 7 (20 mg/L) with ZnO nanopowder [32]. $K_{AO7}$ and $k_c$ values were 0.354 L/mg and 1.99 mg/L/min, respectively. Chakrabarti and Dutta [47] reported that Langmuir adsorption constant of Methylene Blue and Eosin Y was 0.0345 and 0.0859 L/

**Table 2. Kinetics models, electrical energy per order equations and parameters for the photocatalytic degradation of RB5**

| Kinetic models | Electrical energy per order | Parameters |
|---|---|---|
| **Zero-order** $[RB5]_0-[RB5]_t=k_0t$ | $E_{EO}=\frac{38.4\times P}{V\times k_{obs}}$ | $[RB5]_0$ (mg/L), $[RB5]_t$ (mg/L), $k_0$ (mol $L^{-1}$ $min^{-1}$), $k_{obs}$ (1/min), $k_2$ (L $mol^{-1}$ $min^{-1}$), $[RB5]_0$ (mg/L), $k_c$ (mg$L^{-1}$ $min^{-1}$), $K_{RB5}$ (L $mg^{-1}$), P (kW), V (L), $E_{Eo}$ (kWh/$m^3$) |
| **First-order** $\ln\frac{[RB5]_0}{[RB5]_t}=k_{obs}t$ | $E_{EO}=\frac{p\times t\times 1000}{V\times 60\times\log([RB5]_i/[RB5]_f)}$ | |
| **Second-order** $\frac{1}{[RB5]_0}-\frac{1}{[RB5]_t}=k_2t$ | | |
| Langmuir-Hinshelwood $-\frac{d[RB5]}{dt}=\frac{k_cK_{RB5}[RB5]}{1+K_{RB5}[RB5]_0}=k_{obs}[RB5]$ | | |
| $\frac{1}{k_{obs}}=\frac{1}{k_cK_{RB5}}+\frac{[RB5]_0}{k_c}$ | | |

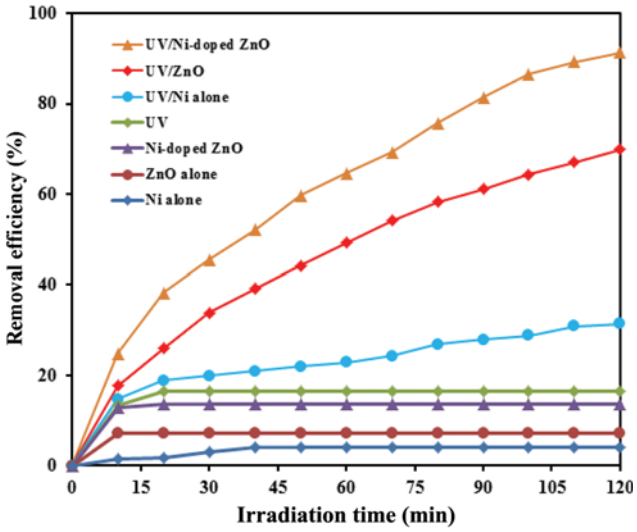


**Fig. 13. The contribution of each process involved in the photocatalytic degradation of RB5 (catalyst dosage=0.2 g/L, pH=7, $[RB5]_0$=20 ppm).**

mg, respectively, from the photocatalytic degradation of two textile dyes using ZnO [47]. $E_{Eo}$ values for the processes studied in this work are summarized in Table 3. $E_{Eo}$ value increased from 39.34 to 941.18 kWh/m$^3$ with increasing RB5 concentration from 5 to 100 mg/L.

## 4. The Comparison of Each Process

To evaluate the effect of various processes on the photocatalytic degradation of RB5, the removal efficiency of RB5 by Ni-alone, ZnO-alone, Ni-doped ZnO, UV-alone, UV/Ni, UV/ZnO, and UV/Ni-doped ZnO was compared at the same reaction condition. Initial RB5 concentration, photocatalyst dosage, and initial pH were 20 mg/L, 0.2 g/L, and 7, respectively. Fig. 13 shows that the removal efficiency for each process was 4.17%, 7.2%, 13.54%, 16.53%, 31.37%, 69.91%, and 91.35%. The removal of RB5 through just adsorption process was insignificant. As shown in Fig. 13, RB5 removal through just adsorption process by Ni-doped ZnO is greater than ZnO-alone. This result can be explained by the different adsorption capacity due to different surface properties, including surface morphology. Removal efficiency of RB5 by UV/Ni-doped ZnO process was about 91.35%, which was greater than that by UV/ZnO (69.91%) process. Removal efficiency difference between UV/Ni-doped ZnO and UV/ZnO-alone is greater than that between Ni-doped ZnO and ZnO-alone. This comparison shows that the UV/Ni-doped ZnO process is an effective process for the removal of RB5 from aqueous solution compared to ZnO/UV or UV process. Similar to this study, Amisha et al. [2] performed photo mineralization of RB5 ($5\times10^{-4}$ M) with ZnO using solar and UV-A light at pH7 [2]. They reported that ZnO-alone just removed 8.68% of RB5 through adsorption process. They also reported that RB5 removal by ZnO/solar light and ZnO/UV was 52.5% and 99.91%, respectively.

The $E_{Eo}$ values for UV, UV/Ni, UV/ZnO, and UV/Ni-doped ZnO rods processes are summarized in Table 4. The $E_{Eo}$ value of UV/Ni-doped ZnO rods process is lower than that of UV, UV/Ni, and UV/ZnO processes. Daneshvar et al. [32] reported $E_{Eo}$ values

**Table 4. The $E_{Eo}$ values for photolytic and photocatalytic degradation of RB5 (catalyst dosage=0.2 g/L, $[RB5]_0$=20 ppm and pH=7)**

| Process | $E_{Eo}$ (kWh/m$^3$) |
|---|---|
| UV | 15297.79 |
| UV/Ni | 2643.43 |
| UV/ZnO | 571.7 |
| UV/Ni-doped ZnO | 265.53 |

of 384 and 172 kWh/m$^3$ from the photodegradation of Acid Orange 7 by UV/ZnO and UV/ZnO/$H_2O_2$ processes, respectively [32].

The mechanism for the photocatalytic removal of dye was reported by Senapati et al. [50]. When Ni-doped ZnO is illuminated with the UV light ($\lambda$<390 nm), an electron excites from the valence band to the conduction band to give electron-hole pairs (Eq. (6)) [51]:

$$ZnO+h\upsilon \rightarrow ZnO\ (e^-_{CB}+h^+_{VB}) \quad (6)$$

Then, electron and hole can take part in the reactions with electron acceptors like $O_2$ and donors like $H_2O$ or $OH^-$ to generate highly reactive radical species like hydroxyl radicals ($E^0$=+3.06 V) [51].

$$h^+_{VB}+RB5 \rightarrow RB5^{\bullet+} \rightarrow \text{oxidation of the RB5} \quad (7)$$

$$h^+_{VB}+H_2O \rightarrow H^+ + \bullet OH \quad (8)$$

$$h^+_{VB}+OH^- \rightarrow \bullet OH \quad (9)$$

$$\bullet OH+RB5 \rightarrow \text{degradation of the RB5} \quad (10)$$

In general, the doping of a metal ion in a semiconductor shifts the Fermi level towards more negative potentials and improves the efficiency of the interfacial charge transfer process [52]. Therefore, electron transfer can occur from the conduction band of ZnO to the new Fermi level (Ef) in the Ni/ZnO structure [53]. From this result, the photodegradation of RB5 by Ni/ZnO hybrid can be enhanced due to the production of more hydroxyl radical in comparison to pure ZnO. In addition, the photogenerated electrons in the new Fermi level can be easily trapped by the adsorbed $O_2$ [50]. From this reaction, superoxide radicals are produced and form $HO_2$ in the presence of water [50]. Subsequently, $HO_2$ is reduced to $H_2O_2$, followed by the generation of hydroxyl radical, the main species to bring about the degradation of dye molecules as follows [50].

$$O_2+e^- \rightarrow \cdot O_2^- \quad (11)$$

$$\cdot O_2^- + H^+ \rightarrow HO_2\bullet \quad (12)$$

$$HO_2\bullet + e^- + H^+ \rightarrow H_2O_2 \quad (13)$$

$$H_2O_2+e^- \rightarrow OH\bullet + OH^- \quad (14)$$

## 5. Spectral Changes of RB5 During Photocatalytic Degradation and Reusability of Catalyst

The changes in the absorption spectra of RB5 solutions during the photocatalytic process at different irradiation times are shown in Fig. 14. The spectrum of RB5 in the visible region exhibits a main band at 597 nm. The decreased absorption peak of RB5 at

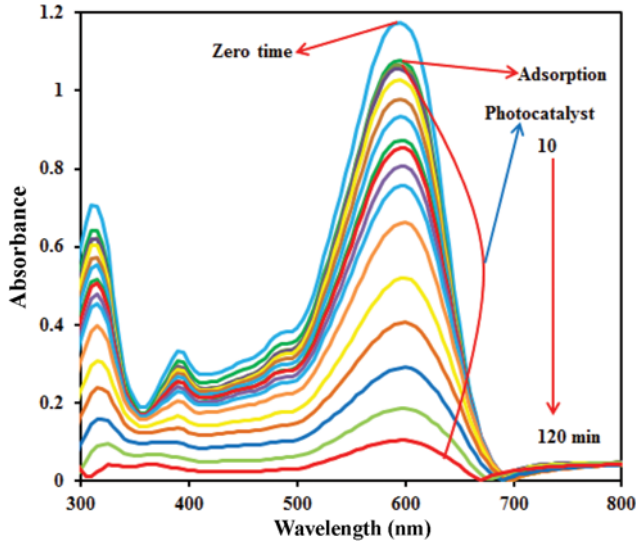


**Fig. 14. Spectral changes of RB5 solution during illumination in the presence of Ni-doped ZnO (catalyst dosage=0.2 g/L, pH =7, $[RB5]_0$=20 ppm).**

597 nm indicates a rapid degradation of the dye molecule. It also indicates that a nitrogen double bond (-N=N-) of the azo dye is the most active site for oxidative attack. Near complete degradation of the dye was observed after 2 h in an optimized condition [2,9,18]. The reusability of the photocatalyst for the photocatalytic degradation of RB5 was measured by applying five repeated cycles of photocatalytic reaction and desorption process (Fig. 14). The photocatalytic degradation of RB5 was performed with an initial concentration of 20 mg/L, catalyst dosage of 0.2 g/L at pH 7. It was observed that photocatalytic degradation of RB5 decreased from 91.35 to 65.4% without any desorption with NaOH at the second cycle. Then, the photocatalyst loaded with pollutant was placed in the 2 M NaOH solution as a desorbing agent. As can be seen in Fig. 15, Ni-doped ZnO showed same photocatalytic activity during five consecutive runs.

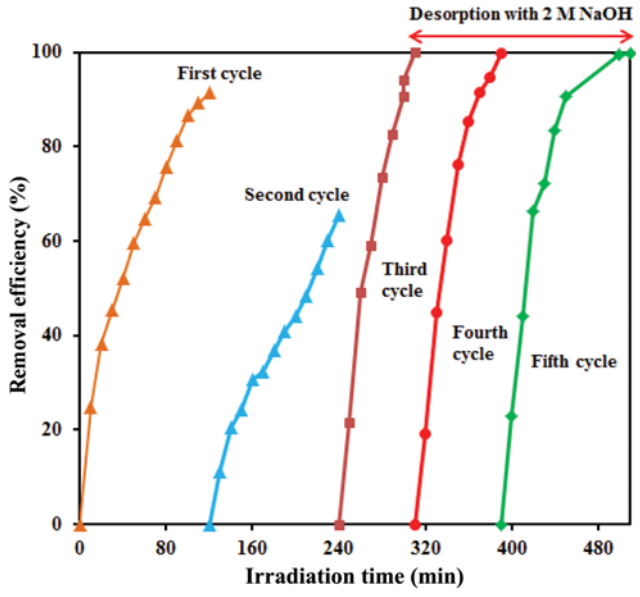


**Fig. 15. Reusability test for the photocatalytic degradation of RB5 within five repeated cycles (catalyst dosage=0.2 g/L, pH=7, $[RB5]_0$=20 ppm).**

## CONCLUSIONS

ZnO rods were doped with nickel through a simple co-precipitation method and their photocatalytic activity for the degradation of an azo dye was assessed. The prepared Ni-doped ZnO rods were characterized by FT-IR, XRD, FE-SEM, and EDX analyses. XRD analysis showed crystallized nature of ZnO with pure wurtzite phase. UV/Ni-doped ZnO rods showed the greatest photocatalytic activity compared with other processes. As the nanocatalyst dosage increased, the photocatalytic degradation of RB5 increased. Maximum degradation efficiency was observed at neutral pH because of the photo-corrosion of Ni-doped ZnO rods as well as electrostatic repulsions at exceedingly low and high pH values. By first-order kinetic assumption, the kinetic rate and the L-H adsorption constants were determined as 0.241 L/mg and 0.524 mg/L/min, respectively. The electrical energy consumption per order of magnitude for photocatalytic degradation of RB5 by UV/ZnO-$TiO_2$ process was lower than that by UV/ZnO, UV/Ni, and UV process. The removal efficiency of RB5 was increased with purging gases and addition of hydrogen peroxide compared to that at ambient condition. The presence of organic compounds such as humic acid, EDTA, oxalic acid and phenol hindered the photocatalytic degradation of RB5. However, it increased in the presence of folic acid and citric acid, which can produce additional oxidant during photocatalytic degradation of RB5.

## ACKNOWLEDGEMENT

This paper is issued from an integrated research of 93-02-27-24803 as a project number PhD student project of Mehdi Shirzad-Siboni. Financial support was provided by Iran University of Medical Sciences, Iran.

## REFERENCES

1. M. Ahmadi, P. Amiri and N. Amiri, *Korean J. Chem. Eng.*, **32**, 1327 (2015).
2. S. Amisha, K. Selvam, N. Sobana and M. Swaminathan, *J. Korean Chem. Soc.*, **52**, 66 (2008).
3. G. Ciobanu, M. Harja, L. Rusu, A. Mocanu and C. Luca, *Korean J. Chem. Eng.*, **31**, 1021 (2014).
4. K. Mahmoudi, K. Hosni, N. Hamdi and E. Srasra, *Korean J. Chem. Eng.*, **32**, 274 (2015).
5. G. Panthi, M. Park, H.-Y. Kim, S.-Y. Lee and S.-J. Park, *J. Ind. Eng. Eng. Chem.*, **21**, 26 (2015).
6. M. S. Lucas and J. A. Peres, *Dyes Pigm.*, **71**, 236 (2006).
7. M. Shirzad-Siboni, A. Khataee, F. Vafaei and S. W. Joo, *Korean J. Chem. Eng.*, **31**, 1451 (2014).
8. M. Muruganandham, N. Sobana and M. Swaminathan, *J. Hazard. Mater.*, **137**, 1371 (2006).
9. I. A. Şengil and M. Özacar, *J. Hazard. Mater.*, **161**, 1369 (2009).

10. M. Shirzad-Siboni, A. Khataee and S. W. Joo, *J. Ind. Eng. Chem.*, **20**, 610 (2014).
11. I. Koyuncu, *Desalination*, **143**, 243 (2002).
12. Y. Liu and D. Sun, *J. Hazard. Mater.*, **143**, 448 (2007).
13. S.-A. Ong, L.-N. Ho, Y.-S. Wong and K. Raman, *Water. Air. Soil Pollut.*, **223**, 1615 (2012).
14. Y. Na, S. Song and Y. Park, *Korean J. Chem. Eng.*, **22**, 196 (2005).
15. S. I. Dorovskikh, S. V. Trubin, E. S. Filatov, V. V. Kriventsov, S. G. Kozlova, Y. V. Shubin, N. B. Morozova and I. K. Igumenov, *J. Phys. Chem. Solids*, **74**, 1204 (2013).
16. B. Thongrom, P. Amornpitoksuk, S. Suwanboon and J. Baltrusaitis, *Korean J. Chem. Eng.*, **31**, 587 (2014).
17. E. C. Ilinoiu, R. Pode, F. Manea, L. A. Colar, A. Jakab, C. Orha, C. Ratiu, C. Lazau and P. Sfarloaga, *J. Taiwan. Inst. Chem. Eng.*, **44**, 270 (2013).
18. S. Chaudhari, A. Bodade and G. Chaudhari, *Korean J. Chem. Eng.*, **30**, 2001 (2013).
19. Y. Kim, J. Lee, H. Jeong, Y. Lee, M.-H. Um, K. M. Jeong, M.-K. Yeo and M. Kang, *J. Ind. Eng. Chem.*, **14**, 396 (2008).
20. R. Darvishi Cheshmeh Soltani, A. Rezaee and A. Khataee, *Ind. Eng. Chem. Res.*, **52**, 14133 (2013).
21. R. D. C. Soltani, A. Rezaee, A. R. Khataee and M. Safari, *J. Ind. Eng. Chem.*, **20**, 1861 (2014).
22. T. Kumpik, W. Thongsuwan and P. Singjai, *Thin. Solid. Films*, **516**, 5640 (2008).
23. J. Zhao, L. Wang, X. Yan, Y. Yang, Y. Lei, J. Zhou, Y. Huang, Y. Gu and Y. Zhang, *Mater. Res. Bull.*, **46**, 1207 (2011).
24. S. Kant and A. Kumar, *Adv. Mat. Let.*, **3**, 350 (2012).
25. K. Raja, P. Ramesh and D. Geetha, *Spectrochim. Acta. A. Mo.l Biomol. Spectrosc.*, **120**, 19 (2014).
26. P. Saharan, G. R. Chaudhary, S. Lata, S. Mehta and S. Mor, *Ultrason. Sonochem.*, **22**, 317 (2015).
27. K. Vignesh, M. Rajarajan and A. Suganthi, *J. Ind. Eng. Chem.*, **20**, 3826 (2014).
28. R. Elilarassi and G. Chandrasekaran, *Optoelectron. Lett.*, **6**, 6 (2010).
29. A. Patterson, *Physical Review*, **56**, 978 (1939).
30. N. V. Kaneva, D. T. Dimitrov and C. D. Dushkin, *Appl. Surf. Sci.*, **257**, 8113 (2011).
31. C.-J. Chang, C.-Y. Lin and M.-H. Hsu, *J. Taiwan. Inst. Chem. Eng.*, **45**, 1954 (2014).
32. N. Daneshvar, M. H. Rasoulifard, A. R. Khataee and F. Hosseinzadeh, *J. Hazard. Mater.*, **143**, 95 (2007).
33. N. Daneshvar, D. Salari and A. R. Khataee, *J. Photochem. Photobiol., A*, **162**, 317 (2004).
34. M. Shirzad Siboni, M. T. Samadi, J. K. Yang and S. M. Lee, *Environ. Technol.*, **32**, 1573 (2011).
35. M. Shirzad-Siboni, M. Farrokhi, R. Darvishi Cheshmeh Soltani, A. Khataee and S. Tajassosi, *Ind. Eng. Chem. Res.*, .**53**, 1079 (2014).
36. W. Horwitz, Editor, Standard Methods for the Examination of Water and Wastewater, 20th Ed., APHA, Washington, DC (2000).
37. M. Shirzad-Siboni, A. Khataee, B. Vahid, S. W. Joo and S. Fallah, *Curr. Nanosci.*, **10**, 684 (2014).
38. A. Bokare, M. Pai and A. A. Athawale, *Sol. Energy*, **91**, 111 (2013).
39. M. Rajendraprasad Reddy, V. Supriya, M. Sugiyama and K. Reddy, Eds. Physical Investigations on ZnO: Ni Layers Deposited by Spray Pyrolysis. Conference Papers in Science; 2013: Hindawi Publishing Corporation.
40. J. Iqbal, B. Wang, X. Liu, D. Yu, B. He and R. Yu, *New. J. Phys.*, **11**, 063009 (2009).
41. S. Husain, F. Rahman, N. Ali and P. Alvi, *J. Optoelectron. Eng.*, **1**, 28 (2013).
42. N. Daneshvar, S. Aber, M. S. Seyed Dorraji, A. R. Khataee and M. H. Rasoulifard, *Sep. Purif. Technol.*, **58**, 91 (2007).
43. J. Miao, Z. Jia, H.-B. Lu, D. Habibi and L.-C. Zhang, *J. Taiwan. Inst. Chem. Eng.*, **45**, 1636 (2014).
44. X. Cai, Y. Cai, Y. Liu, H. Li, F. Zhang and Y. Wang, *J. Phys. Chem. Solids*, **74**, 1196 (2013).
45. A. Jonidi-Jafari, M. Shirzad-Siboni, J.-K. Yang, M. Naimi-Joubani and M. Farrokhi, *J. Taiwan. Inst. Chem. Eng.*, **50**, 100 (2015).
46. A. Mohagheghian, S.-A. Karimi, J.-K. Yang and M. Shirzad-Siboni, *J. Adv. Oxid. Technol.*, **18**, 61 (2015).
47. S. Chakrabarti and B. K. Dutta, *J. Hazard. Mater.*, **112**, 269 (2004).
48. B. Pare, P. Singh and S. Jonnalgadda, *Indian J. Chem., Sect A*, **48**, 1364 (2009).
49. J. K. Yang, S. M. Lee and M. Shirzad-Siboni, *Environ. Technol.*, **33**, 2027 (2012).
50. S. Senapati, S. K. Srivastava and S. B. Singh, *Nanoscale*, **4**, 6604 (2012).
51. M. Qamar and M. Muneer, *Desalination*, **249**, 535 (2009).
52. V. Subramanian, E. E. Wolf and P. V. Kamat, *J. Am. Chem. Soc.*, **126**, 4943 (2004).
53. R. Georgekutty, M. K. Seery and S. C. Pillai, *J. Phys. Chem. C*, **112**, 13563 (2008).